LLNL-TR-813279

Lawrence Livermore National Laboratory

Magnetic Microcalorimeter Gamma Detectors with Ultra-High Energy Resolution

FINAL REPORT

webPMIS number

Stephan Friedrich

07/25/2020

Disclaimer

Lawrence Livermore National Laboratory is operated by Lawrence Livermore National Security, LLC, for the U.S. Department of Energy, National Nuclear Security Administration under Contract DE-AC52-07NA27344.

Table of Contents

Section 1

Summary

Objective

The goal of this project was to build a commercially viable metallic microcalorimeter (MMC) γ-spectrometer with an ultra-high energy resolution <50 eV for accurate non-destructive assay (NDA) of nuclear materials. Improved NDA simplifies and accelerates safeguards analyses in the nuclear fuel cycle and enhances capabilities to detect the diversion of nuclear materials for illicit purposes. High-resolution MMC γ-spectrometers can also improve the accuracy of nuclear data that NDA is based on.

Tasks

There were the major sets of tasks for this project:

1.) First and foremost was the goal to **design and fabricate magnetic microcalorimeter (MMC) γ-detectors with an energy resolution <50 eV**, an order of magnitude better than conventional Ge detectors. This involved introducing new sensor materials, optimizing detector geometries and scaling the optimized design to 32-pixel arrays. The detectors were fabricated at STAR Cryoelectronics LLC to **establish a commercial source of MMCs**.

2.) The second task was to enable **continuous, ultra-high resolution MMC operation by non-expert users** in preparation for commercialization. This required purchasing a liquid-cryogen-free dilution refrigerator with a base temperature <10 mK and adapting it for MMC operation.

3.) The final task was to **demonstrate the instrument's capabilities** with ultra-high resolution γ-spectra from safeguards-relevant samples. The goal was to help make MMCs commercially viable by showing potential customers specific results of interest to them.

Results

The design, fabrication and testing of MMC γ-detectors went through three iterations: Single-pixel devices in the first year, 14-pixel test arrays in the second year, and 32-pixel MMC detector arrays in the final year. The detectors used erbium-doped silver (Ag:Er) as the magnetic sensor material, a thick electroplated gold (Au) γ-absorber and a novel passive heat switch in the magnetization circuitry. We developed extensive MMC modeling capabilities and used them to design and analyze MMCs with the SQUID preamplifier integrated on the same chip and on separate chips. The final MMC γ-spectrometer used a 32-pixel array with four separate SQUID chips to read out the γ-ray signals (Figure 1) [Boyd 2020]. The MMCs were operated in a liquid-

cryogen-free dilution refrigerator at a temperature of ~15 mK and have achieved an energy resolution as high as 37 eV at 60 keV (Figure 2) [Boyd 2018].

We have used the MMCs to demonstrate high-resolution γ-spectroscopy of various actinides of interest in nuclear safeguards and have started to quantify isotope analysis. This includes measurements on Th-234 [Friedrich 2018], U-233 [Kim 2018a] and weapons-grade Pu. One crucial (and often underappreciated) result was that we observed the *same* deviations from the literature values with *different* sets of MMCs designed and fabricated by *different* groups and read out with *different* amplifier chains. This further supports the observation that MMCs have an intrinsically more reproducible response than other cryogenic detector technologies.

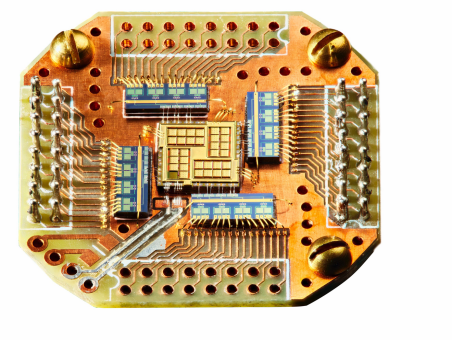

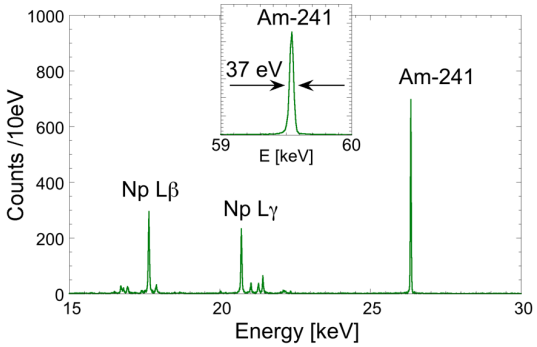

Figure 1 (left): Picture of a 32-pixel MMC γ-detector array (center) surrounded by four blueish SQUID preamplifier chips [Boyd 2020]. Figure 2 (right): High-resolution γ-ray spectrum of an Am-241 test source [Boyd 2018].

Outlook

With the completion of this project, the basic MMC γ-detector technology is in place and ready for use in experiments. Photolithographic Ag:Er MMC fabrication at a small company is established, including the integration of thick electroplated absorbers. SQUID preamplifiers for MMC readout are commercially available, and so are the "dry" dilution refrigerators to operate MMCs at temperatures down to ~10 mK without using cryogenic liquids.

By no means does this imply that no further development is desirable. One limitation of MMCs at this point is that the device fabrication and performance is not yet sufficiently reliable and uniform for a commercial product. In addition, the software for data acquisition and pulse processing is custom-written and not as user-friendly as desirable. Finally, detector performance can still be improved, especially with regards to count rate capabilities.

I expect future advances to be more closely related to specific scientific and programmatic questions. We have e.g. recently been funded to use MMCs to accurately (re)measure the controversial half-life of Sm-146, an important isotope for early solar system chronometry. We are also in discussions with LANL about using MMCs to accurately measure the total kinetic energy (TKE) of fission in Cf-252, a crucial reference material for calibration of neutron detectors and neutron multiplicity. Finally, we are currently setting up an SP-1 with the IAEA to develop MMC decay energy (Q) spectrometers for isotope analysis of small particles. I have no doubt that there will be plenty of other opportunities that make use of the unique properties of MMCs.

Section 2

Description of Work by Tasks

Task 1: MMC Detector Development

Conceptually, the design and operating principle of MMC γ-detectors are relatively simple: They consist of an absorber optimized for the radiation of interest that is attached to a paramagnetic sensor in a magnetic field at low temperature (Figure 1). Gamma-ray absorption changes the temperature of the absorber in proportion to the γ-energy, and the resulting change in sensor magnetization $\chi \propto 1/T$ (Curie susceptibility) is read out with a SQUID preamplifier.

In practice, MMC γ-detectors are sophisticated devices whose geometries and materials need to be carefully optimized and whose photolithographic fabrication requires state-of-the-art facilities and materials that are often not commercially available. The absorber needs to be at least several 10s of μm thick for efficient gamma-ray absorption, which cannot be done by sputter deposition and requires the integration of an electroplating process for absorber fabrication. The ideal paramagnetic sensor material is erbium-doped silver (Ag:Er), which is not commercially available. The sensor material needs to be magnetized at temperatures of ~10 mK with currents above 100 mA that require a high-quality Nb magnetization coil. A secondary coil in close proximity to the Ag is required to efficiently pick up the magnetic signal, and the layered multi-coil structure must be free of electric shorts. The detector must be able to cool down quickly to the cryostat temperature to increase the count rate capability. Spatial variations of the detector response must be minimized for high energy resolution, and the response of different pixels must be uniform across the detector array to allow summing the signals from different pixels (Figure 2).

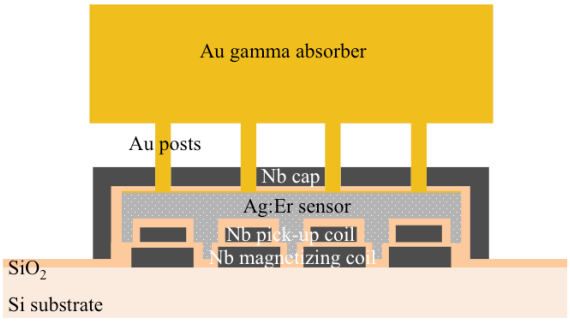

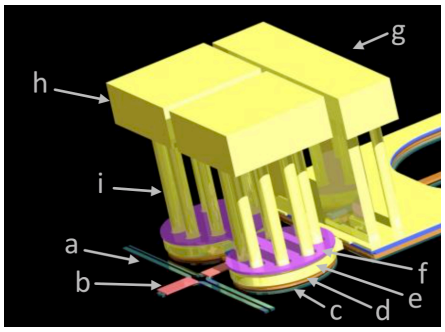

Figure 1 (left): Schematic cross-section of an MMC gamma detector (not to scale). The thick electroplated γ absorber is supported on top of the paramagnetic Ag:Er sensor by Au posts. The lower Nb coil is used to magnetize the sensor, and the upper coil is used to pick up the signal and couple it to the SQUID preamplifier. Figure 2 (right): A 3D schematic of an MMC shows the magnetizing circuit (a), the heat switch (b) to trap the current in the magnetizing coil (c), the sensing coil (d) below the paramagnetic Ag:Er sensor (e), the superconducting Nb cap (f) to confine the magnetizing filed to the sensor (e), and the Au absorber (h) supported on Au posts (i, with height greatly exaggerated for clarity) on top of the sensor. The thermal bus (g) is designed to efficiently cool the MMC back to the base temperature of the cryostat [Boyd 2018].

Despite these technical challenges, MMCs are being developed world-wide for various scientific and programmatic applications. The primary reason is their ultra-high energy resolution, which is an order of magnitude higher than for conventional Ge detectors and therefore overcomes line overlap problems, especially at low γ energies. But in addition, MMC have the advantage among cryogenic detector technologies that they are thermal equilibrium detectors with a reproducible and in detail predictable response, so that spectra from different pixels can be calibrated with a simple quadratic polynomial and added without loss in energy resolution or change in line shape. This is crucial for high-accuracy measurements. Demonstrating the reproducibility and predictable response of MMCs had been the most important result of our predecessor project LL12-MagMicro-Pd03 [Bates 2016b]. This report summarizes the technology development of the successor project LL16-MagMicro-PD2La and the improvements in MMC γ-detector performance they have enabled.

Simulations of Detector Response

We have performed extensive simulations of the MMC detector response at the Center for Supercomputing at the University of New Mexico. These simulations included the full 3D geometry of the MMC (Figure 2) and covered the frequencies into the GHz range that had to be included due to the ac Josephson effect in the tunnel junctions of the preamplifier SQUID.

One question was how to efficiently and uniformly couple the B-field to the paramagnetic Ag:Er sensor without exceeding maximum (critical) current of the superconducting Nb magnetizing coil. The solution was to cover the Ag:Er sensor with a superconducting Nb cap, which excludes magnetic fields due to the Meissner effect and thereby confines the field to the volume of the Ag:Er sensor (Figure 1). A related question was how to design the magnetizing coil to ensure a uniform magnetic flux. Since there is a trade-off between the cross section of the Nb coil and thus its critical current, the number of turns required for a desired magnetic field and the fabrication difficulty and thus the device uniformity and yield, several iterations were required to arrive at a final design (Figure 3).

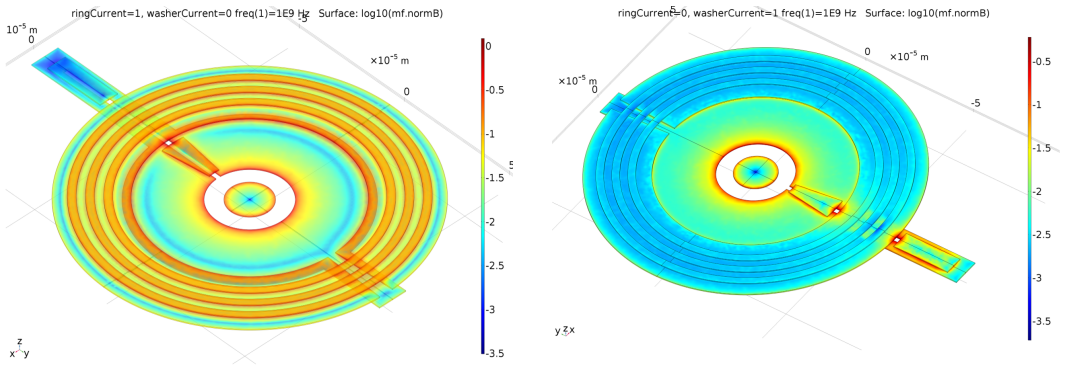

Figure 3 (left): Simulated magnetic fields at the surface of the magnetizing coil, here simplified to three concentric loops (right), and in the SQUID sensor coil (left). Understanding the surface fields helps us to spot and eliminate unintended flux concentrations. Because these calculations are fully 3D, they allow us for the first time to accurately account for non-axisymmetric features such as the leads, a flux-concentrating washer added to reduce capacitive coupling, and three patches added to reduce slit inductance.

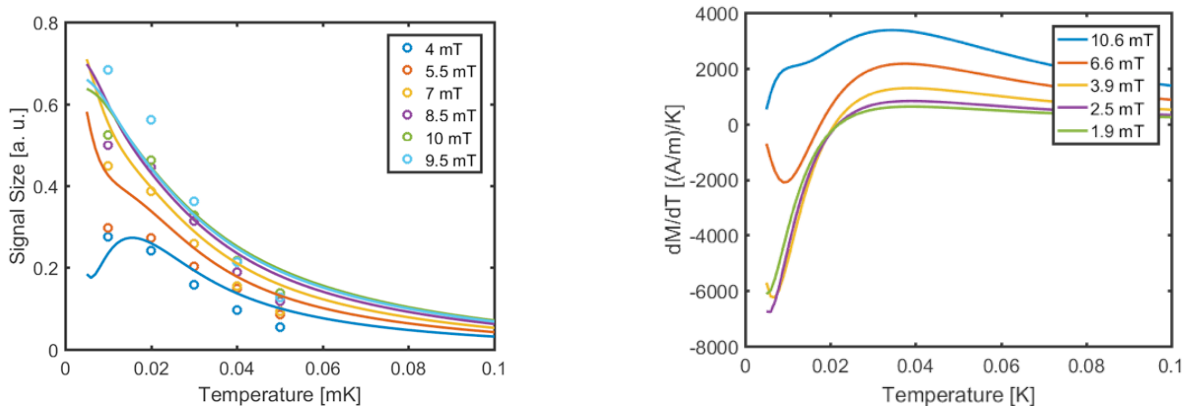

Figure 4 (left): Simulation of gamma signal size as a function of temperature for different applied magnetic fields (solid lines), compared to the values measured in one of our first-generation Ag:Er MMCs (circles). These simulations are used to extract the exact device parameters such as heat capacities, thermal conductivities and coupling constants. Figure 5 (right): Simulations for a particular MMC geometry illustrate that the magnetic sensor response to gamma-ray heating (dM/dT) depends sensitively on temperature and applied magnetic field (different colors). Detector optimization is therefore a complicated iterative process constrained by photolithographic capabilities.

We have also modeled the MMC signal and its dependence on device parameters extensively (Figure 4). These models included simulations of parasitic capacitances and inductances due to the geometry of the design. One difficulty is that heat capacities and thermal conductances can often only be approximated initially, because the properties of sputtered polycrystalline films can differ from the literature values of pure high-quality materials. In addition, the magnetic coupling and thus the signal size depends sensitively on the actual thickness of the SiO_2 insulator between the magnetic Ag:Er sensor and the Nb pick-up coil (Figure 1). We have therefore typically integrated several different device geometries in the same test arrays, so that we could compare the response of neighboring pixels where only a single device parameter was changed and identify the reason for differences between simulations and measurements. Measured signal sizes for different magnetic fields B and temperatures T (Figure 4, circles) were then fed back into the simulations to optimize the MMC design. Figure 5 illustrates that this was not a trivial task given how sensitively the responsivity of an MMC can depend on B and T.

At the end of this project, we now have a significant set of numerical tools to model MMC γ detectors. They can be used to understand and optimize their performance, and to adapt MMC designs to different types of radiation and optimization goals [Boyd 2018 and 2020].

Paramagnetic Erbium-Doped Silver

Our earlier MMC detectors had used erbium-doped gold (Au:Er) as the paramagnetic sensor material [Bates 2016a, 2016b]. While the performance was acceptable, the magnetic quadrupole moment of the Au-197 nucleus added undesirable heat capacity to the system and caused the MMC signal to display an overshoot at the beginning of the pulse (nicknamed the "gold nose" in the MMC community). Erbium-doped silver (Ag:Er) was predicted to provide better performance as a sensor material, because its two isotopes Ag-107 and Ag-109 have spin-1/2 nuclei without a quadrupole moment, and we had therefore proposed to develop Ag:Er-based MMCs as part of this project.

Since Ag:Er is not commercially available, we had to produce the Ag:Er sputtering targets for photolithographic MMC fabrication ourselves. The difficulties are 1) that Er must be distributed uniformly throughout the Ag to prevent ferromagnetic ordering of the Er spins at low temperatures (which would render them useless as magnetic sensors), and 2) that Er must be prevented from oxidizing to maintain its paramagnetic properties. To address these challenges, we have built a setup to heat metallic high-purity Ag and Er under UHV conditions above the melting temperature of Ag while rotating the mixture to distribute the Er dopants uniformly throughout the Ag (Figure 6). The dilute "solid solutions" of Er are then characterized magnetically to confirm the total erbium concentration of ~800 ppm and the absence of ferromagnetic ordering, and if the samples meet specs, they are machined with non-magnetic tools into 1" sputtering targets (Figure 7). This process development also had to go through several iterations until we had learned to control all relevant details and could produce the Ag:Er sensor material with the right properties reliably. The result is the development of MMCs whose signals decay with a single exponential decay constant (Figure 8). While this sounds trivial, it is unusual for cryogenic microcalorimeters, whose signals typically have multiple decay constants that change slightly with γ-ray energy. That prevents the use of simple and fast trapezoidal filtering algorithms and greatly complicates the use of optimum filters, which require a constant signal shape. In contrast, we can process our MMC signal with simple fast trapezoidal filters that can be easily integrated into a commercial system.

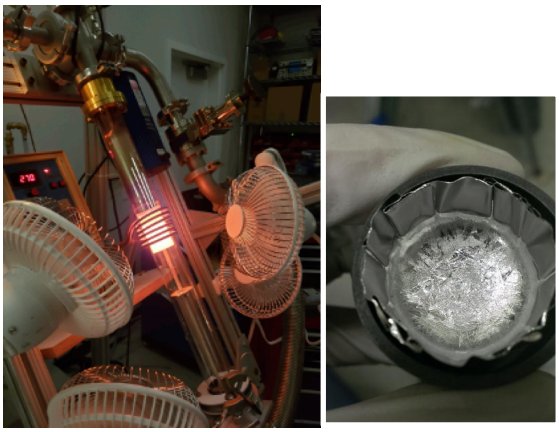

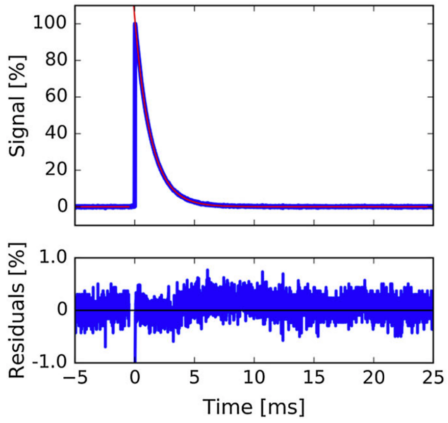

Figure 6 (left): Rotating UHV induction furnace for Ag:Er target fabrication at UNM. Figure 7 (center): Ag:Er sample from the furnace to produce a 1" diameter sputtering target. Figure 8 (right): In contrast to earlier Au:Er MMCs (and to TES microcalorimeters), the pulse shape of our Ag:Er MMCs has a single exponential decay constant [Kim 2018a].

Electroplated Gold Absorber on Posts

While the thin films of the magnetic sensors, the superconducting Nb coils and the SQUID preamplifiers can be sputter-deposited using standard processes at STAR Cryoelectronics, γ detectors require absorbers with a thickness of at least several ~10s of μm that are too thick for fabrication by sputtering. We therefore had to develop an electroplating process that could integrate a thick Au absorber with a photolithographically-defined sensor structure. An additional difficulty was that the absorber could not be electroplated directly onto the Ag:Er sensor underneath, because high-energy phonons produce during the initial thermalization of the γ energy would escape into the substrate and produce a low-energy tail below each line. Instead, we had shown in our predecessor project that the absorber needed to be supported on posts that serve as a thermal bottleneck between Au absorber and Ag:Er sensor, so that the γ energies are thermalized uniformly in the absorber before heating the sensor (Figure 1, 2) [Bates 2016b].

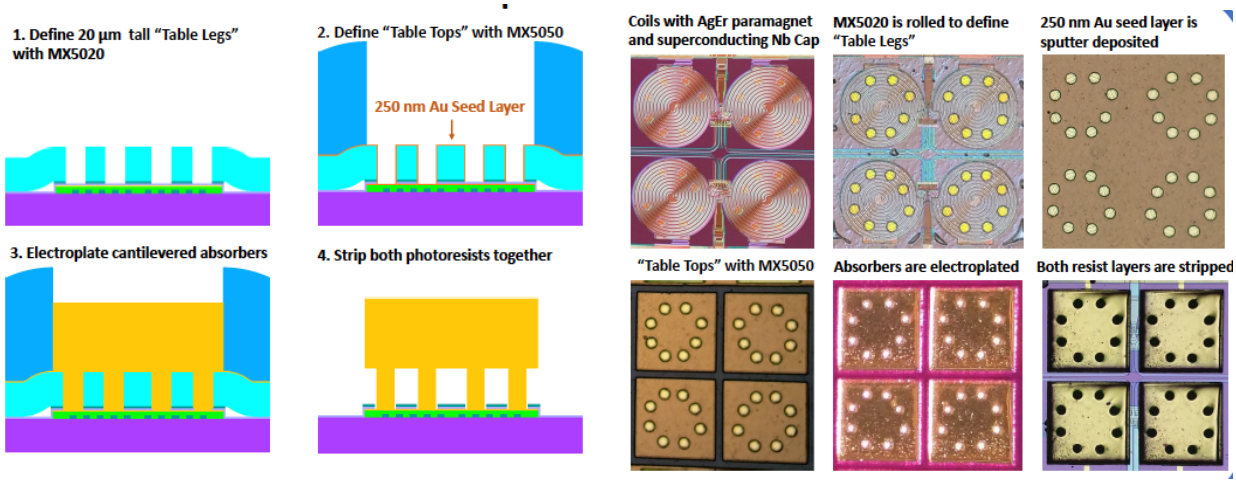

Figure 9 (left): Schematic of the absorber fabrication process using two different photoresists (light and dark blue) to define the "legs" (or "posts") and the "top" of the gold absorber. Figure 10 (right): Top view of four absorbers in an MMC detector array on top of the circular pick-up coil and paramagnetic sensor during the corresponding stages of fabrication [Hummatov 2018].

We have developed a process to from a mold for electroplated Au absorbers using two types of thick roll-on photoresist (Figure 9). The first type of photoresist (DuPont MX-5020) has a thickness of 20µm and is rolled directly onto the MMC sensor structure. It is patterned by exposure to UV light and developed chemically just like standard photoresist to form the pattern of the absorber posts. We use eight posts with 50 µm diameter in a circular pattern to support the absorber and ensure uniform coupling between absorber and Ag:Er sensor. The second roll-on photoresist (DuPont MX-5050) has a thickness of 50 µm and different chemical properties, so that it can be exposed to UV and patterned without affecting the pattern in the first layer. Its pattern determines the area of the absorber. Before electroplating the absorber into the mold, the contact area to the sensor is cleaned by plasma etching and a 250 nm thick Au seed layer is deposited by sputtering to ensure good mechanical and thermal contact between Au absorber and Ag:Er sensor. The absorber is then deposited by electroplating at a constant current in a custom-designed rig with agitation of the solution to ensure uniform absorber deposition and the desired thickness. Stripping both layers of photoresist then produces the cantilevered absorber on top of the Au posts. Figure 10 shows four of MMC pixels from one of the arrays during the various stages of the absorber fabrication [Hummatov 2018]. As for the other technical developments of this project, this process emerged as the most reliable one after multiple other approaches had been tested and rejected.

Heat Switch

For a typical data acquisition over several hours, it is important that the magnetizing field of the sensor remain constant. This is accomplished by trapping a persistent current in the Nb coil underneath the sensor. For this, the Nb coil consists of a loop with a superconducting heat switch that can be heated into the normal state without driving the entire coil normal (see Figure 2). The magnetizing current is applied to the coil from an external source while the heat switch is normal and resistive, and when the heat switch is then cooled back into the superconducting state, the current is trapped in the loop and the external source can be turned off. In the past, the heat switch typically contained a heater that allowed raising the heat switch temperature temporarily above T_C. However, repeated operation of this heater would damage the switch until it eventually failed.

We had therefore proposed to develop a passive heat switch with a critical temperature above that of liquid helium so that it could be heated with the entire detector stage of the cryostat during cooldown but would remain superconducting during a magnetization cycle of an ADR cryostat. For this, we had initially investigated Nb/Ta bilayers whose Nb/Ta ratio we could adjusted to produce the desired transition temperature (far left in Figure 11). While this approach worked, the properties of the Nb/Ta bilayer depended on the details of the interface and were therefore difficult to reproduce reliably [Hummatov 2017]. We eventually settled on a heat switch made from a NbTa alloy whose composition we chose to provide a critical temperature $T_C = 5.2$ K. We showed that such a NbTa alloy can sustain persistent currents >200 mA indefinitely and have used this design of a heat switch for all later versions of our MMCs [Boyd 2018].

Single pixel MMCs

To ensure that the MMCs of this project would be commercially viable, we had decided early on to fabricate all MMC detectors at STAR Cryoelectronics LLC and base our designs on their fabrication capabilities. One difficulty was that it is quite expensive to produce a full 4" wafer of devices, and that a full 4" wafer contains many more detectors than are needed for the R&D stage of a project where process parameters still need to be optimized. We therefore decided to fabricate only the Nb coils, wiring, heat switches and SQUID preamplifiers on the full 4" wafer scale, because the fabrication processes for these components were well-established and could be done reliably with high yield. We then diced the 4" wafer into many ~1 cm^2 chips and did the R&D steps of this project on these smaller chips. This reduced the number of expensive production runs of 4" wafers and allowed using small Ag:Er targets that we could fabricate in our current induction furnace (Figure 6). We could also use the small dedicated sputtering system for Ag:Er film deposition that UNM had developed during the preceding project [Jaeckel 2012].

Figure 11 shows some of the details of the first single-pixel MMCs we made with Ag:Er. These detectors were still crude, and their initial resolution was "only" 150 eV. But they allowed us to test the quality of the first paramagnetic Ag:Er material we had made and the fundamental soundness of our approach. Subsequent simulations and MMC detector designs were based on the materials parameters we extracted from these devices during the first year of the project.

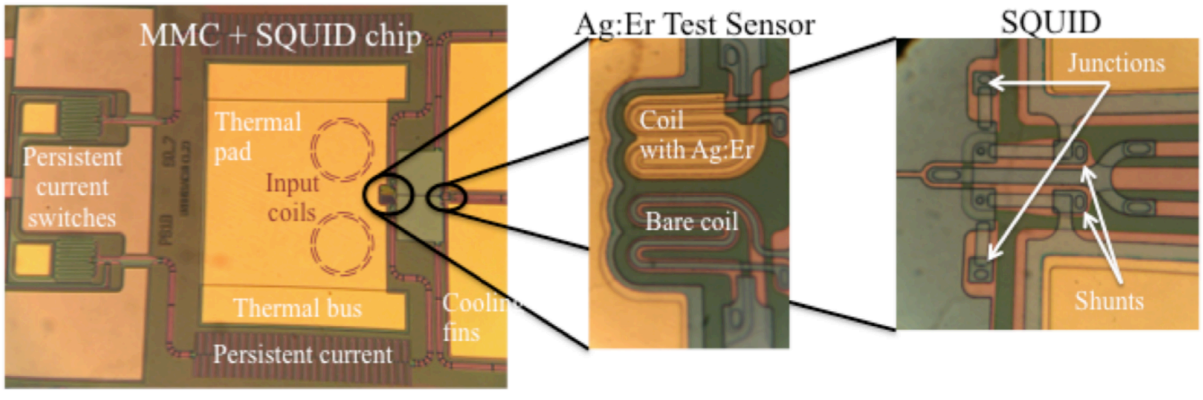

Figure 11: Details of the initial single-pixel MMC Ag:Er γ-detectors that we used to confirm the viability of Ag:Er as a sensor material and to extract material parameters of the films used in our MMC design. Note that the SQUID preamplifier is integrated on the same chip as the MMC.

14-Pixel Test Array

The MMC γ-detector arrays we built in the second year of this project served two purposes: to improve the performance over the single-pixel devices based on the material parameters we had extracted, and to explore different new design ideas that we had developed theoretically but never tested experimentally. All designs integrated the SQUID and sensor on the same chip as the MMC and use a superconducting Nb cap layer on the paramagnet to confine the magnetic field, but they explore different combinations of combined/separate sensing and magnetization coils and direct/flux transformer coupling to the input SQUIDs. Integrating SQUID and MMC on the same chip allows optimal inductance matching and control of stray reactances. The designs explored different combinations of one-layer/two-layer sensing coils and direct/flux transformer coupling of the input circuits [Boyd 2018]. We also tested different widths of the gold path to cool the MMC back down to the base temperature of the cryostat to see whether we could speed up the MMC response without loss in energy resolution.

As before, we fabricated all the Nb magnetization coils, wiring, heat switches and SQUID preamplifiers in a single fabrication run on a 4" wafer. This 4" wafer was then diced into many ~1 cm^2 chips that were processed individually to try out different deposition conditions and optimize the properties of the Ag:Er paramagnet and the thickness of the SiO_2 insulator between the Ag:Er and the pick-up coil (a crucial parameter!), the Nb cap and the electroplated Au absorber. A scanning electron microscope (SEM) image of the completed detector array is shown in Figure 12. The inset shows how the square Au absorber makes contact to the Ag:Er sensor underneath only at the eight circular posts that serve as a bottleneck to ensure uniform thermalization of the gamma-ray energy. The thermal bus is made from the same high-purity (RRR = 30) electroplated gold as the absorber and ensures (relatively) fast transfer of the gamma energy to the thermal bath of the cryostat. A photograph of the array mounted on a chip holder for measurements in shown in Figure 13. Multiple superconducting Al wirebonds are needed to apply up to 150 mA of magnetizing current to the Nb coils at 10 mK without heating the chip. Wirebonds for thermal contact are made from gold, which does not have insulating oxides on its surface and does not turn superconducting even at the lowest temperatures and there for retains its high thermal conductivity.

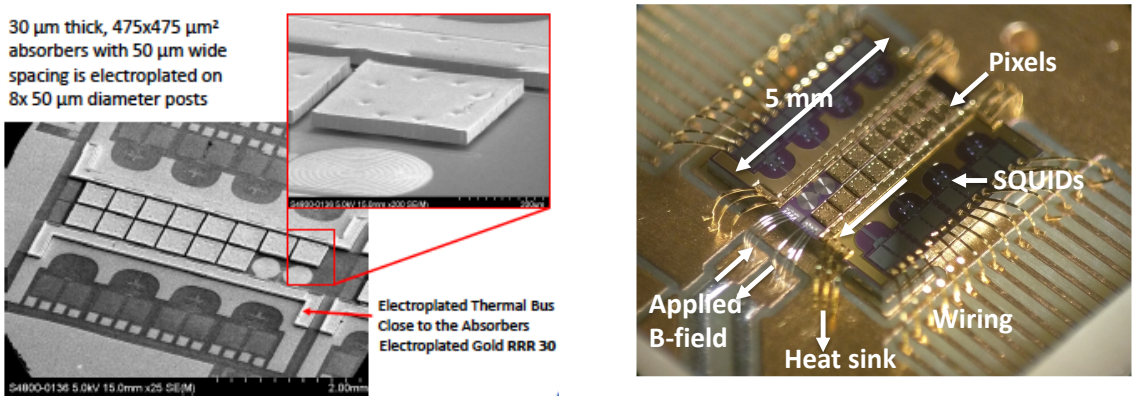

Figure 12 (left): Electron microscope (SEM) picture of the detector array. The 14 squares in the center are 14 gamma-ray absorbers, and the two round pick-up coils on the right are SQUID thermometers for on-chip temperature regulation. The inset shows the thick Au absorber supported on 8 Au posts. Figure 13 (right): The array chip mounted on a ceramic chip holder for testing. The wire bonds at the top and bottom make contact to the first-stage SQUID pre-amplifiers, the Al wire bonds are used to apply the magnetizing current, and the gold wire bonds on the left and right sides of the chip ensure good thermal contact of the detectors to the cryostat for fast thermalization and (relatively) high detector speed.

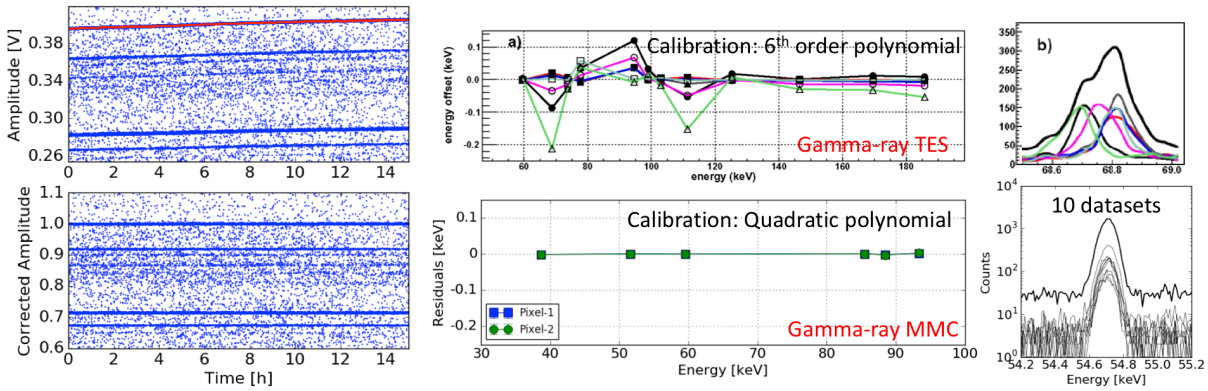

Fig. 14 (left): A scatter plot of the γ-induced events over a period of 15 hours shows that the pulse amplitudes change due to small temperature drifts (top). They can be corrected (bottom) by normalizing the data by a moving average over a strong line at high energies (red). Fig. 15 (right): An important advantage of MMCs over superconducting transition edge (TES) microcalorimeters is their simple quadratic response function. This simplifies calibration (center) and ensures that spectra from different pixels line up even between the calibration points, so that they can be added without loss in resolution or distortion of the pulse shape [Bates 2016b, Kim 2018b]. The plot shows the residual deviation of the measured centroids from the calibrated value (center) and the line shape of the spectral sum (right).

The MMCs were tested in our dilution refrigerator as a function of magnetization current, temperature, gamma-ray energy and SQUID bias. We measured pulse amplitudes, rise and decay times and noise spectra under various condition to compare them to the models (see figures 4 and 5), to better understand the physics of the devices and to optimize detector performance. One observation was that, although the temperature of the dilution refrigerator was regulated, almost all signals showed some drift in their amplitudes over typical time scale of hours (Figure 14). This was due to small drifts in the array temperature relative to the cryostat base temperature. We can correct for this drift by calculating a moving average over a strong line at high energy (Figure 14, red line) and normalizing all events by this average.

After this drift correction, the MMC spectra can be calibrated with a simple second-order polynomial (Figure 15). This is not a trivial result. In fact, this simple quadratic response function is a crucial advantage of MMCs over superconducting transition edge (TES) microcalorimeters, whose spectra must be calibrated with a higher-order polynomial that differs between pixels and (for the same pixel) between runs (Figure 15). The simple calibration of MMCs was one of the most important results of the predecessor proposal [Bates 2016], and the results from this proposal show that this was not an exception for a few select MMCs but is fundamentally related to the different sensor technologies. MMCs are based on temperature changes of the Curie susceptibility of the magnetic erbium ions, which is a thermodynamic equilibrium quantity. In contrast, TESs are based on the resistive phase transition between the superconducting and the normal state of the sensor, which is intrinsically less reproducible in detail and exhibits small irregular structure. This causes TESs to require a higher-order polynomial for energy calibration, and even then the spectra between the calibration points to not always line up accurately, so that TES peaks can be broadened and lose their Gaussian shape (Figure 15, right). Spectra from MMCs, on the other hand, are repeatable and mostly linear, with a small but reproducible quadratic correction, and can be added without loss in energy resolution (Figure 15, right) [Bates 2016, Kim 2018a].

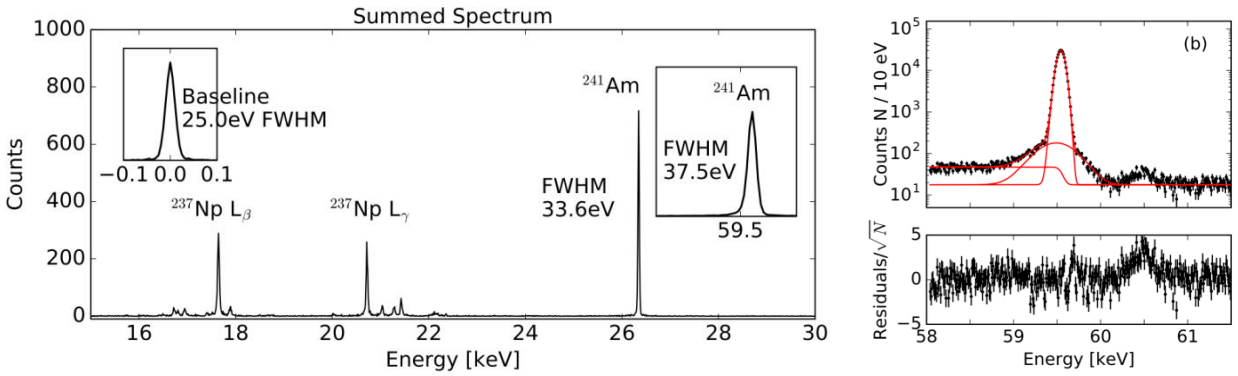

Fig. 16 (left): High-resolution spectrum of an Am-241 source taken with the MMC gamma-ray detector in Figure 13. Fig. 17 (right): The MMC response is Gaussian on top of a step background due to small angle scattering between source and detectors. In addition, there is a small distribution of events due to pile-up of pulses with dual polarity. The peak at 60.5 keV is an escape line.

The highest-resolution MMC γ-spectra were taken with a set of MMCs at a magnetizing current to 95 mA to avoid quenching the magnetizing circuit due to heating in the resistive pin connections (see Figure 13). Although the temperature of the cryostat was regulated at 10 mK, we estimate that the detector was likely operating around ~20 mK because the MMC signal stopped increasing below that temperature. This is likely due to heating by the first-stage SQUID that is integrated on the same chip as the MMC and the Kapton insulation between the detector holder and the mixing chamber that we added to reduce electromagnetic interference. The Am-241 source was external to the cryostat and irradiated the detector through thin windows. The MMC input SQUID was read out with a STAR Cryo AR232-16 SQUID array amplifier and PFL-102 readout electronics, then low- pass filtered with 1 MHz bandwidth. The filtered signals were sampled at 2 MSa/s with a 16-bit GaGe digitizer. Six-millisecond-long waveforms were processed by a trapezoidal filter using a 0.9-ms peaking time and a 2.5-μs gap time. The positive-going and negative-going signals from the two gradiometric MMC sensors were linearly separately, and the two spectra were then summed to produce the spectrum in Figure 16 [Boyd 2018]. At the time, the energy resolution of 37.5 eV FWHM was the world's best energy resolution for MMC γ-detectors (although recently our collaborators in Heidelberg have improved the design of their MMCs and shown better results).

The MMC response function is well described by a Gaussian function on top of a step-function due to small angle scattering in the shielding between the source and the detector (Figure 17). In addition, we see a second Gaussian function that is smaller and broader and depends on the count rate we operate the detector at. It is due to pile-up between pulses of different polarity, since two MMC pixels are read out with the same SQUID preamplifier in our gradiometric design.

Ge-Detector Compton Veto

One general limitation of all microcalorimeter detectors is that their very high energy resolution requires a small pixel volume of order ~1 mm^3. This limits the efficiency of γ-detection and restricts their use to γ energies below ~100 or ~200 keV depending on design. This is often acceptable, because most line overlap problems occur for low-energy γ-rays, and high-accuracy NDA of actinides in nuclear safeguards applications are based on γ-rays in the 100 keV range. Still, many gamma-rays cannot be detected with microcalorimeters.

To address this limitation, we had proposed to operate a conventional high-purity Ge detector at ~10 mK directly behind the MMC array. This Ge would extend the energy range of the instrument into the MeV range, because most high-energy γ-rays would be transmitted through the MMC and detected by the Ge detector. In addition, it could serve as a Compton veto to reject events from γ-rays that were forward-scattered in the MMC and thereby generate a low-energy background. A hybrid detector with an MMC array in front and Ge detector behind it would combine the strengths of both technologies: The MMC provides ultra-high energy resolution and a low background at low energies where the sensitivity of Ge detectors can be limited by line overlap and the Compton background, and the Ge provides high efficiency over the full MeV range of γ-energies where line overlap is less of a problem and Compton backgrounds are lower.

This is the only task of this project that we have not been able to implement successfully. We had successfully operated at Ge detector in our adiabatic demagnetization refrigerator (ADR) at temperatures down to ~0.1 K and expected them to be no different in the dilution refrigerator at 10 mK. We were aware that the Ge detector response at ultra-low temperatures changes over time due to carrier freeze-out and had expected to address this problem by periodically exposing the Ge detector to photons from an LED. However, the dilution refrigerator we set up for MMCs uses a pulse tube refrigerator for precooling to ~3 K instead of liquid N_2 and He precooling in our ADR. This introduces significant amount of electromagnetic interference. For MMC operation, we had made sure that the MMC were well-shielded and electrically isolated from ground. For the Ge detector, we used existing mounting scheme that made electrical contact to one of the Ge electrodes. The electromagnetic pick-up was tremendous, and simple changes we made to the grounding and shielding did not suppress it significantly. With the time and resources we had for this project, we could not re-design the Ge detector mount and had to abandon this task.

We do not believe that there is any fundamental reason that Ge detectors cannot be operated at ~10 mK and serve as a Compton veto and energy range extender for MMC γ-detectors. Various Ge detectors cooled to ~100 K by a pulse tube refrigerator are commercially available whose energy resolution is not much worse than that of nitrogen-cooled Ge detectors. And various experiments (such as the cryogenic dark matter search CDMS) have been operating Ge detectors at 10 mK for years, as long as they periodically fill trap states by exposing the Ge crystal to LED light. In fact, we still think that a hybrid MMC / Ge detector is a great idea, and we hope that we will be able to implement it as part of a future project.

32-Pixel Arrays

The final 32-pixel array of MMC γ-detectors is shown in Figure 18. Design parameters and geometries were fine-tuned, and due to our experience of MMC heating in the 14-pixel arrays, where MMCs and SQUIDs had been integrated on the same chip, we decided to separate MMCs and SQUID onto different chips connected by superconducting Al wire bonds. Future designs might still use an integrated design, which can ultimately provide better performance, but for now we felt we should follow the safer approach [Boyd 2020]. As before, the Nb magnetization coils, wiring and the SQUID preamplifiers were fabricated one a full 4” wafer, which was then cut into ~1 cm^2 chips to add the Ag:Er sensor and the Au absorber. We increased the thickness of the absorber to 50 µm, sacrificing highest energy resolution for increased γ-detection efficiency. Unexpectedly, two of the four final 32-pixel arrays had an open circuit in the Nb magnetization coil whose cause we still do not quite understand, indicating that even minor changes in design can sometimes affect the performance of parts of the circuitry that is well established.

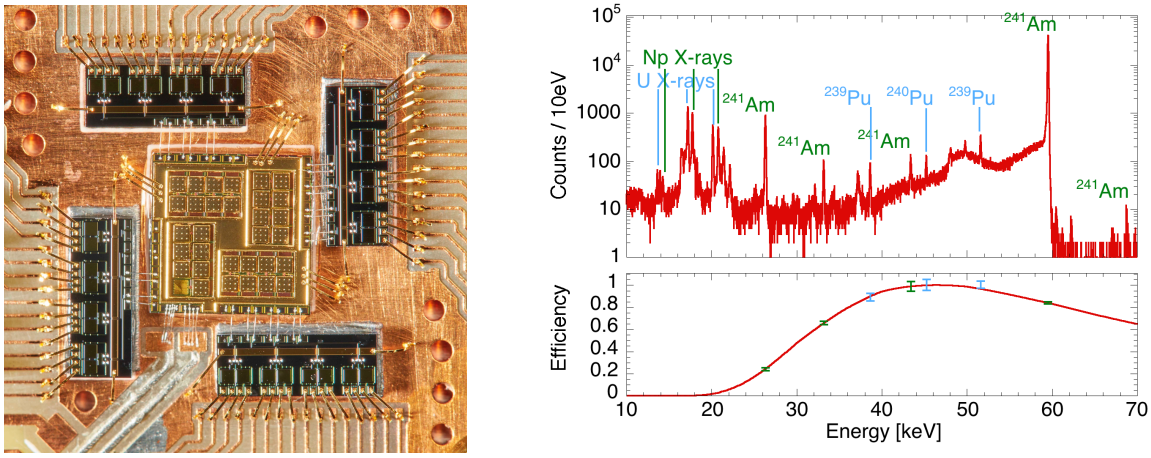

Figure 18: Close-up of a 32-pixel MMC γ-detector array mounted on a printed-circuit board (PCB) for operation. The central array consists of four groups of 2 x 8 MMC pixels (the pixel on the lower left does not have a Au absorber and can be used as an on-chip thermometer) that are wire-bonded to four separate SQUID preamplifier chips. The magnetizing current is provided to the Nb coils under the MMCs through the two superconducting solder-coated wires and Al wire bonds on the lower left. Au wire bonds from the MMC to the Cu ground plane of the PCB (which extends to the back side of the PCB though Cu-plated vias) provide the thermal path for cooling to the cryostat temperature. Figure 19 (right): MMC sum spectrum of a WGPu source shows the gamma emissions from the three dominant isotopes in the sample. The four Am-241 gamma-emissions can be used to extract an efficiency curve at low energies.

We prepared a special source of weapons-grade plutonium (WGPu) with known isotopic composition to test the performance of the array. At this point, we had mostly run out of time and funding, so we could only test four of the 32 pixels. (As usual, we had underestimated the number of detailed problems that we had to overcome during fabrication and when trying to integrate a Ge Compton veto with the MMC ay 10 mK.) An Al filter was placed between the WGPu and the MMC to reduce the intensity of the L X-rays to avoid exceeding the count rate of the detector. The full signal waveforms were written to disc and processed off-line with a trapezoidal filter. The amplitudes were drift-corrected with a moving-average window over the strong Am-241 line at 60 keV. The spectra were calibrated individually with a quadratic fit to the Am-241 γ-lines and summed (Figure 19, top). The sum spectrum has an energy resolution of ~100 eV, more than sufficient to separate all lines of interest. It is dominated by the strong Am-241 γ-ray at 60 keV as expected, with γ-emissions from Pu-239 and Pu-240 and X-ray peaks of their Np and U daughters visible at low energies.

To test the feasibility of quantitative analysis, we have extracted the efficiency curve η(E) of our MMCs from a fit to the known branching ratios of the Am-241 γ-emissions (Figure 19, bottom). Since MMCs are small and multiple-scattering inside the MMC is negligible, η(E) can be described accurately as a function of the energy E with an analytical expression that accounts for the self-absorption in the source and attenuation in the Al windows between source and MMC:

$$\eta(E) = \eta_0 \left(\frac{1-e^{-\mu_{Pu}(E)d_{Pu}}}{\mu_{Pu}(E)d_{Pu}}\right) e^{-\mu_{Al}(E)d_{Al}}\left(1 - e^{-\mu_{Au}(E)d_{Au}}\right) \qquad (1)$$

The term in the first brackets in Equation (1) describes the self-absorption of the radiation in the WGPu source, the second term the attenuation in the Al windows with total thickness d_{Al} between source and detector, and the term in the second brackets the absorption in the Au absorber of the MMC with thickness d_{Au}. The elemental mass absorption coefficients μ_{Pu}, μ_{Al} and μ_{Au} can

be obtained from various data bases, e.g. https://www.nist.gov/pml/x-ray-mass-attenuation-coefficients. The scale factor η_0 accounts for the solid angle that the MMC covers for a particular experimental setup. Equation (1) can be used to fit the measured detection efficiency well within the accuracy of the literature branching ratios for Am-241, with the Au absorber thicknesses slightly adjusted from the nominal design values to account for fabrication uncertainties and variations in density from the literature values. The measured isotope ratio Pu-240/Pu-239 = 6.25(36) % agrees with the specifications for WGPu. So far, this NDA accuracy of ~5.8% is still limited by the statistical uncertainty of the Pu lines due to the low count rate of less than 10 counts/s per pixel and the strong Am-241 line at 60 keV, which dominates the count rate. This again demonstrates the need for MMC arrays and the desire to speed up their response. With improved statistics, it would ultimately be possible to determine this isotope ratio by NDA with an accuracy of 2.2%, currently limited by the uncertainties of the associated branching ratios of 0.0447(9) % and 0.02722(22) % for the strong Pu-240 and Pu-239 lines at 45.244 and 51.624 keV, respectively. Improving these branching ratios and thus the NDA accuracy of the Pu-240/Pu-239 ratio would be possible with MMCs by using the better-known branching ratios of Am-241.

Task 2: Refrigeration

The second set of tasks of this project was to enable continuous, ultra-high energy resolution MMC operation by non-expert users in preparation for commercialization. This required, in particular, the availability of a liquid-cryogen-free ("dry") dilution refrigerator for long-term automated MMC operation at temperatures as low as 10 mK. The low base temperature of a dilution refrigerator, which was not attainable in the adiabatic demagnetization refrigerators (ADRs) we had used in the predecessor project [Bates 2016a, 2016b], was necessary to attain an energy resolution <50 eV FWHM. The desire to attain this performance without the use of liquid helium was based on the goal of subsequent commercialization of MMC detectors through the STTR / SBIR program with STAR Cryoelectronics LLC, the company that was fabricating the MMC detectors for this project.

BlueFors Dilution Refrigerator

Several companies currently sell liquid-cryogen-free "dry" dilution refrigerators with base temperatures around ~10 mK in the price range between ~$300k and ~$500k depending on size and cooling power. Most prominent among them are Oxford Instruments (Great Britain), Janis (USA), BlueFors (Finland) and Leiden Cryogenics (Netherlands). Based on performance specifications and on extensive discussions with colleagues who had experience with different dilution refrigerators, we decided to buy a BF-LD-400 dilution refrigerator from BlueFors Cryogenics (Figure 20). It uses a two-stage pulse tube refrigerator from Cryomech to precool its outer stages to ~55 K and ~3 K, and a closed-cycle He-3/He-4 dilution unit with a large Pfeiffer HiPace 400 turbo pump. It has a guaranteed base temperature of 10 mK and a cooling power of 12 µW at 20 mK. We purchased the option for Level-1 vibration isolation to reduce the coupling of microphonic noise from the compressor of the pulse tube to the MMC. We also had the instrument equipped with different coaxial cables for possible future experiments on microwave multiplexing. We made sure that the compressor and the pumps was electromagnetically isolated from the cryostat and grounded the cryostat to the building ground through a new dedicated low-resistance Cu ground cable.

The MMC detectors at operated one a custom designed holder inside a magnetic shield made from superconducting Nb behind a side port whose windows have been thinned to ensure gamma transmission from an outside source. The detector holder is galvanically isolated from the rest of the cryostat with thin Kapton tape to reduce electromagnetic pick-up. We installed superconducting CuNi-clad NbTi wiring for 32 MMC pixels from the mixing chamber detector stage to 4 K, and non-superconducting phosphor-bronze wire from 4 K to the hermetic feedthrough at 300 K. The MMC signals are read out in pairs with two-stage SQUID preamplifiers from STAR Cryo. The first stage consists of a single low-noise SQUID that is operated as close to the MMCs as possible to reduce parasitic inductances. The second stage is a 16-SQUID array at 4 K (STAR Cryo model AR-232-16). Both SQUIDs are operated in a flux-locked loop (a term used for the negative feedback circuitry used to ensure stable SQUID operation) with a controller at room temperature (STAR Cryo model PFL-102). For the operation of 32 MMX pixels, we have installed 16 of these two-stage SQUIDs and their controllers. SQUID biasing is done with proprietary STAR Cryo software.

Refrigerator Performance

We have been very satisfied with the performance of this dilution refrigerator. It greatly exceeds the performance specifications, which BlueFors has intentionally kept conservative, and reaches a base temperature <7 mK. In fact, we do not even know the exact base temperature, since the thermometer is only calibrated down to 7 mK and often reads “out of range”. The refrigerator attains this base temperature fully automated and without the use of cryogenic liquids over a period of ~1 day (Figure 22). The measured cooling power of the refrigerator, which determines how many wires can be brought to the low-temperature stage and thus how many MMC detectors can ultimately be operated simultaneously, is 20 µW at 20 mK, significantly above the specified minimum of 12 µW (Figure 23). In addition, there are many beautiful and well thought-out design details that make assembly, operation and modification of the refrigerator easy and intuitive. For example, the outer shell at 300 K and the thermal shields at 50 K and 4 K are made from two parts with simple mounting structure (Figure 21), so that the instrument can be taken apart and re-assembled for different experiments by a single person.

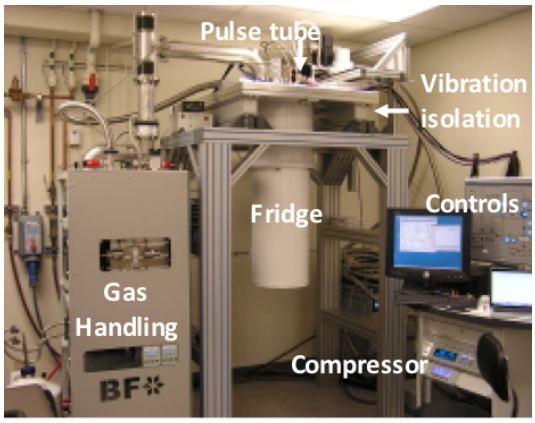

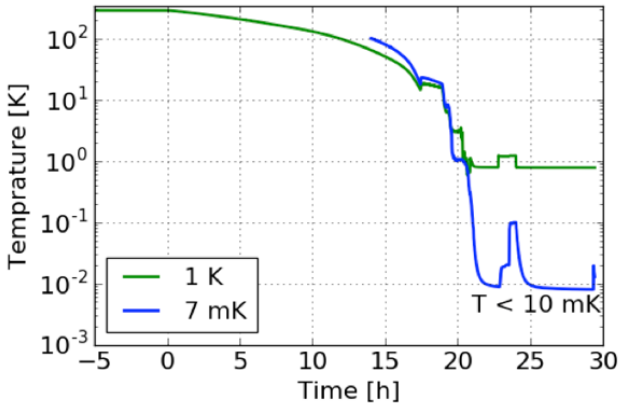

Figure 21 (left): BlueFors BF-LD-400 dilution refrigerator for MMC operation at LLNL. The side port with the re-entrant tube for MMC operation is on the back side facing the wall. Figure 22 (center): Automated cooldown of the dilution refrigerator to its base temperature <10 mK within 24 hours. The green line is the thermometer signal of the still, the blue line is the temperature on the MMC detector stage.

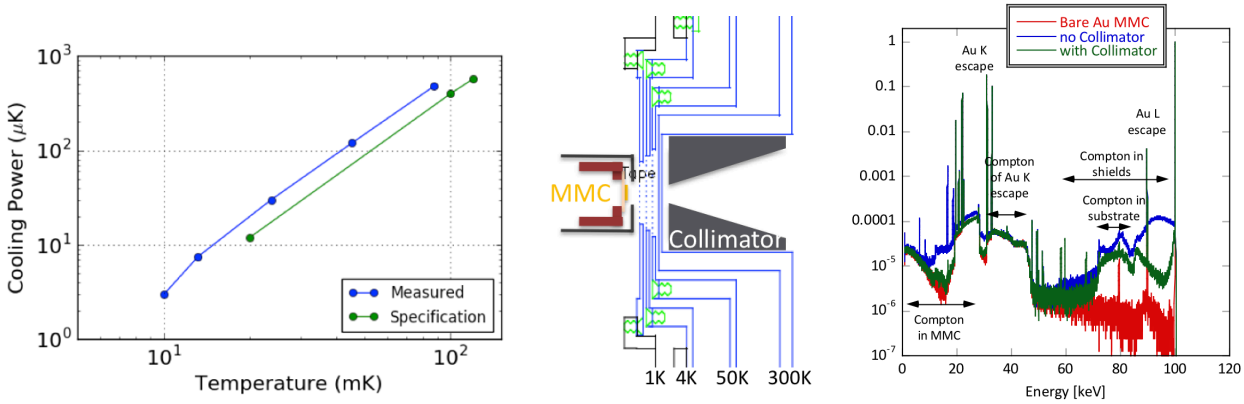

Figure 23 (right): The measured cooling power (blue) exceeds the specified cooling power (green) significantly. Figure 24 (center): Design of the re-entrant tube with thin Al windows (dotted) at the different temperature shields to place a sample to within a few inch of the MMC detector. Figure 25 (right): MCNP simulations show that the Compton background of the MMC spectrum can be kept quite low if the source signal is collimated, the Al windows at the shields are thin and the material surrounding the MMC is minimized.

To bring a radioactive sample outside the refrigerator closer to the small MMC detectors, we have built a 2" diameter "re-entrant tube" with very thin windows at the end to hold a source within a few inches of the MMC array (Figure 24). Monte-Carlo simulations show that with appropriate shielding and windows, the Compton contribution to the spectra can be kept quite low (Figure 25). At some point, it would be desirable to rebuild the sample mount and operate the MMC at the end of a cold finger that extends beyond the cryostat wall to enable the analysis of sources bigger than 2", although there is no immediate need for this.

In summary, our BlueFors dilution refrigerator is easy to operate and works very well, reflecting the careful design and the beautiful cryogenic engineering it is based on. It is a good choice for a commercial MMC γ-spectrometer that requires temperatures well below 50 mK, which are a practical lower limit for ADRs.

Task 3: Applications

Consistency of Response

One of the main motivations to develop MMC detector had always been that they were expected to not only provide ultra-high energy resolution, but also a predictable and reproducible response function. It was one of the most important results of the predecessor project LL12-MagMicro-Pd03 to demonstrate that MMCs do in fact have a response function that is constant between cooldowns and that can be calibrated predictably and to high accuracy with a second-order polynomial [Bates 2016b]. In this project, we had access to two different sets of MMCs, one from the New Mexico and one from Heidelberg (Figure 26), and that has allowed us to test whether reproducibility and quadratic response are just sporadic properties of exceptionally well-built detectors, or whether they are intrinsically related to the operating principle of the MMCs. For this, we asked our radiochemistry colleagues to fabricate a mixed Pu-239 / U-233 source that we could mount at 4 K in front of our MMCs. The Pu-239 γ-emissions were expected to be well-known so that they could be used for energy and efficiency calibration of the MMCs, which could then be used to test the accuracy of the U-233 γ-ray energies and branching ratios. U-233 was chosen because it is fissile currently of interest in the context of the thorium fuel cycle.

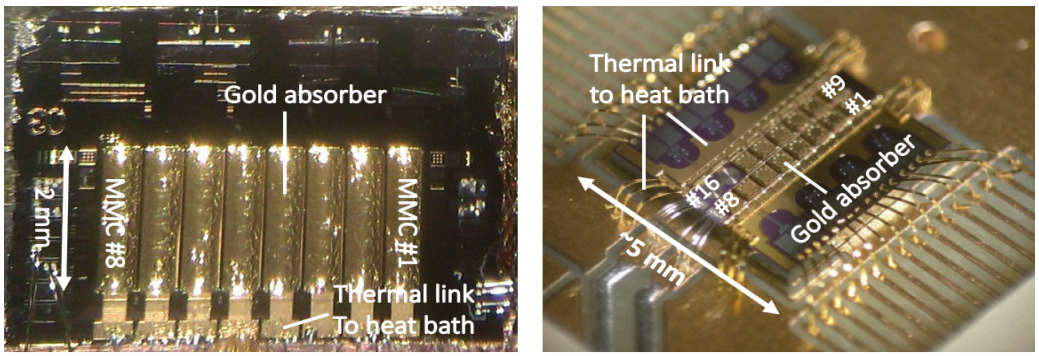

Figure 26: MMC gamma detectors developed at the Kirchhoff Institute of Physics (KIP) at Heidelberg University (left) and at the University of New Mexico (UNM) (right).

Figure 27 (top) shows the spectra of this Pu-239 / U-233 source, measured with the MMC arrays from Heidelberg (green), the MMCs from New Mexico (blue) and with a Ge detector for comparison (red). Using only the strongest γ-rays with the best-known energies, we see that both sets of MMCs can be calibrated over the full range up to 100 keV with a quadratic function, with the second-order term being slightly larger for the smaller New Mexico MMC due to their smaller size and thus larger temperature excursion (Figure 26, middle). Importantly, the residuals, i.e. the deviations of the centroid from their literature value, are the *same* for both sets of MMC, although they were designed and built by *different* groups and read out by *different* SQUID amplifier chains. In fact, *all* centroids agree with one another for the different MMC, although they do not necessarily agree with the NNDC literature values (Figure 28). This suggests that the errors are due to literature values, rather than detector artifacts [Kim 2018b]. This is a big deal.

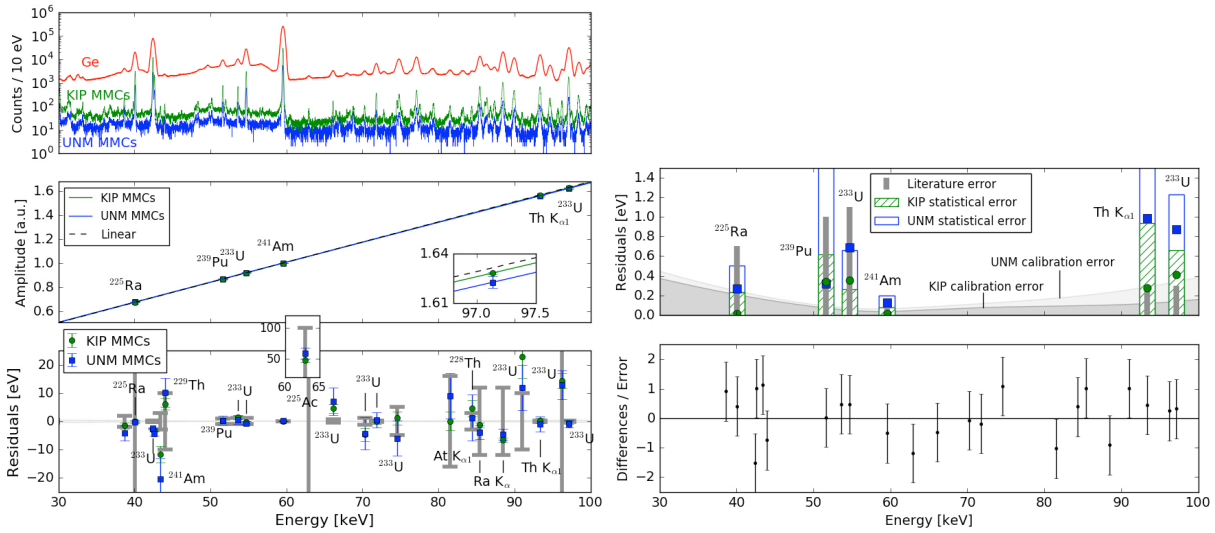

Figure 27 (left): MMC spectra (top), calibration (center) and residuals (bottom) from the same ^{233}U/^{239}Pu source, once measured with MMCs from the Heidelberg Kirchhoff Institute for Physics ("KIP MMCs", green) and once with MMCs from STAR Cryo / U of New Mexico ("UNM MMCs", blue). Both detectors can be calibrated with a simple second-order polynomial, and the non-linearity of the smaller UNM MMCs is larger as expected (center). The residuals for both MMCs agree for all lines within the error of the measurement, suggesting that non-zero deviations from the literature values are due to a literature error rather than detector artifacts. Figure 28 (right): The precision of the MMC measurements is comparable to the precision of the calibration lines in the literature (top). The difference between the UNM and the KIP MMCs are consistent with the error of the measurement for all lines in the spectrum, i.e. the ratio of difference / error is consistent with zero within the error bar of the measurement (bottom) [Kim 2018b].

The fact that the measurements from two *different* MMCs read out by *different* SQUID amplifiers would produce the *same* deviations from literature (Figure 27) is fundamentally the most important result of this project. Among our five presentations, this result received the most (informal behind-the-scenes) praise at the 2019 Workshop on Low Temperature Detectors (LTD-19) in Milan, because it showed not only that we can improve these literature values, but that MMCs can be used for many other measurements that require high precision. This does, of course, not mean that *all* MMCs will *always* produce consistent results –there is still plenty that can go wrong–, but it does show that MMCs are intrinsically suitable for high-precision measurements. In this respect, MMCs provide an advantage over TESs, especially if that the arrays can be scaled to the same number of pixels.

Non-Destructive Assay

We have therefore used the Pu-239 / U-233 spectra to assess the feasibility of quantitative non-destructive assay (NDA) with MMCs. The accuracy of NDA is ultimately limited by the statistical errors due to counting statistics and the systematic errors due to the accuracy of the efficiency calibration and the branching ratios (BRs). The counting statistics are still a problem for MMCs, because we have so far only operated them at a few counts/s per pixel, although this problem is not a fundamental one given that we can fabricate arrays (Figures 18 and 26) and that the signals from different MMC pixels can be added without change in line shape (Figure 15) or loss in energy resolution [Bates 2016b]. Still, statistical uncertainties do currently limit the accuracy of NDA with MMCs (Figure 19).

The more fundamental challenge is how much the systematic errors due to efficiency calibration and branching ratios (BRs) will ultimately limit NDA accuracy with MMCs. For this, we have used the strongest lines in the spectrum with the best-known BRs to determine the quantum efficiency of MMCs with a fit to to Equation (1) (Figure 29). This fit is most accurate in the region between 80 and 25 keV between the K- and L-absorption edges of our gold absorber. We find that the efficiency curve (blue) matches the intensity of the known Pu-239 and Am-241 calibration lines (green) within the accuracy of the literature values (grey). However, even this measurement suggests that the BR of the relatively strong Am-241 line at 43keV is poor.

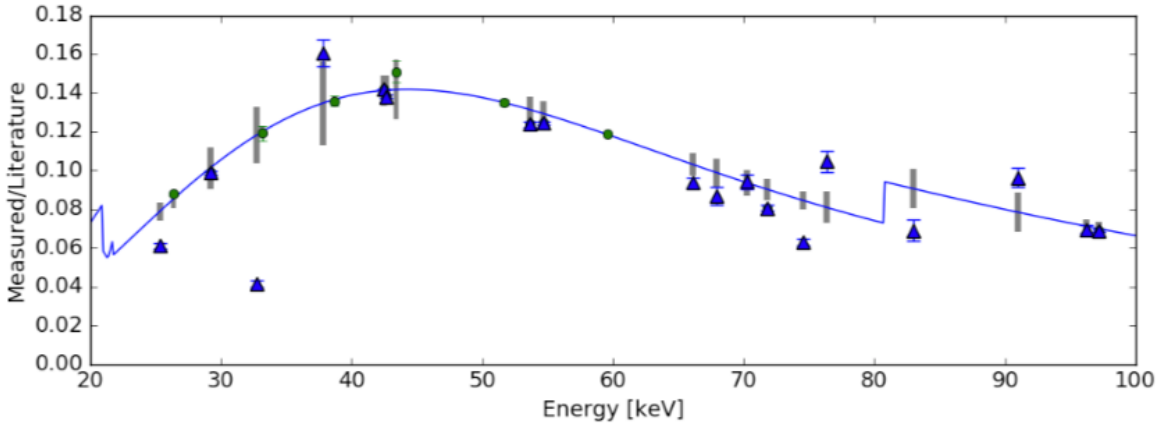

Figure 29: Efficiency calibration (blue) based on the well-known branching ratios of Pu-239 and Am-241 (green markers) according to Equation (1). The measured intensities of the various U-233 γ-rays (blue markers) differ significantly from the NNDC literature values of the branching ratios, whose uncertainties are shown as grey bars.

Interestingly, the measured intensities of the U-233 lines (blue markers) fluctuate widely about the values predicted by the efficiency calibration in Figure 29. Many of the U-233 BR are not very well known, especially at low energy. I suspect that some of the uncertainty is related to the high Compton background of Ge detector at low energy (Figure 27, top) and possible line-overlap that obscures contributions from other isotopes (Figure 30). Based on the nuclear data currently available, we can so far not determine an accurate concentration of U-233 with these measurements for comparison with the known sample composition.

Accurate Nuclear Data

The relatively large data uncertainties for NDA were also emphasized by Alain Lebrun, the Head of the NDA Section of the IAEAs Nuclear Measurement Laboratory (NML), who saw our presentation on MMCs at the NSARD-2018 meeting in Las Vegas and encouraged us to use them to improve nuclear decay data. One example is the measurement of the U-233, whose strong signature at 97 keV was thought to be a triplet of lines. However, the MMC spectra show that one of these lines does not exist (Figure 30). In addition, they indicate the presence of Fr Kβ X-rays due to the decay of U-233 daughter Ac-225 [Kim 2018a]. Lines like these are not visible with Ge detectors, which may contribute to the poor branching ratios for U-233 in the literature.

As a second example, we chose to re-measure the γ-rays of Am-241, whose emission at 59540.9 ± 0.1 eV is one of the best-known γ-energies and is widely used as a low-energy reference, although no systematic errors had been considered in the experiment that this value is based on. We also wanted to examine the limiting factors in the accuracy of MMC spectra. We therefore produced Yb-169 by irradiation of a thulium foil with 15 MeV deuterons at the 88" Cyclotron at LBL, whose γ-emissions have been measured by NIST in the 1980s with a Si double-crystal spectrometer whose lattice constant had been referenced to the definition of the meter. Interestingly, high-resolution γ-spectra of the Yb-169 with and without Am-241 show that the energy of the famous 60 keV line is likely off by a few eV (Figure 31) [Kim 2020]. Measurements like this show the advantages that ultra-high energy resolution, simple energy calibration and a predictable response of MMC can provide.

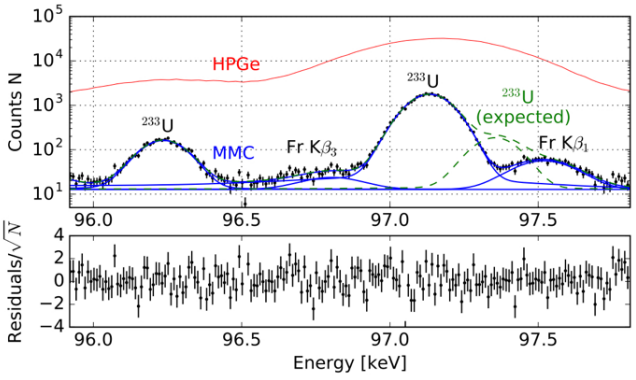

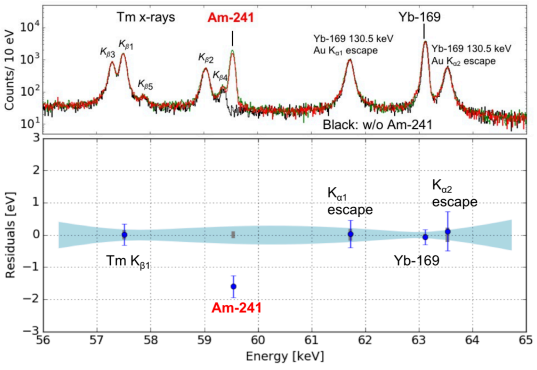

Fig. 30 (left): The 97 keV region of the U-233 / Pu-239 γ-spectrum can be fit (blue) to the data (black) within the statistical accuracy of the measurement (bottom panel). The fit demonstrates that the gamma emissions at 96.22 and 97.13 keV agree with the literature values, but that the postulated line at 97.37(4) keV does not exist [Kim 2018a]. Fig. 31 (right): 60 keV region of an Yb-169 γ-spectrum (top), both with (red, green) and without (black) Am-241. The bottom graph shows the calibration accuracy of the spectrum (blue shade) based on four well-known lines (blue markers), and the deviation of the Am-241 energy from its expected value [Kim 2020].

Section 3

Conclusions and Recommendations

On MMC Technology

With the completion of this project, the **basic MMC γ-detector technology is in place** and ready for use in experiments. Photolithographic MMC fabrication at a small company is established, including the integration of thick electroplated absorbers for (moderately) high efficiency and several other innovations. SQUID preamplifiers optimized to read out MMC signals are commercially available, and so are the "dry" dilution refrigerators to operate MMCs at temperatures down to ~10 mK without using cryogenic liquids. We have demonstrated an energy resolution of 37 eV FWHM, and increased sensitivity by scaling MMCs to 32-pixel arrays. Further improvements in energy resolution are possible, although I do not believe that this would currently provide the most benefits in applications of interest to the NA-22.

By no means does this imply that no further development is desirable. The primary limitation of MMCs at this point is that the device fabrication and performance is **not yet sufficiently uniform and reliable for a commercial product**. After establishing and optimizing the fabrication protocol, we could only fabricate a few complete devices, and their performance is still below the predicted values. For example, the 32-pixel array (Figure 18) may have suffered from incomplete removal of the thick photoresist with a recipe we copied from other groups, which we have recently replaced with a much more reliable recipe. SBIR funding for MMCs would be very desirable to increase detector reliability and user-friendliness.

Similarly, although electronic noise problems kept us from implementing a **Ge detector behind the MMC detector at 10 mK**, we still consider this an excellent idea, because such a Ge detector would not only extend the range of MMC but also serve as a Compton veto to further reduce their low-energy background due to forward-scattered γ-rays. We hope to be given another chance to implement this idea at some point. In addition, the **software** for the data acquisition and the pulse processing electronics **is custom-written and not as user-friendly** as desirable.

Finally, MMC γ-detector performance can still be improved, especially with regards to **count rate capabilities and quantum efficiency**. Many of the NDA measurements are still limited by the total number of counts in the lines of interest, and although this can always be compensated for with larger arrays and longer data acquisition time, there are practical limitations that limit the usefulness of these approaches.

Still, even with the few counts/s per detector pixels, **MMCs can already enable some of the most precise γ-ray measurements ever**. Operating all 32 pixels of the array simultaneously will soon reduce many data acquisition time to acceptable values. This project has established the basic technology and its advantages. I now expect –just like with Ge detectors– decades of incremental improvements.

On MMC Applications

With the basic MMC technology established, I **expect future advances to be more closely related to specific scientific and programmatic questions**. These can be measurements with the γ-ray MMCs of this project, or the adaptation of MMC technology for other types of radiation.

For example, the γ-ray MMC development by our collaborators at Heidelberg University were motivated by the desire to accurately measure the energy levels in Th-229 in order to build a nuclear clock with an unprecedented accuracy of 1 part in 10^{19}. At LLNL, we have recently been funded to use MMCs to accurately (re)measure the controversial half-life of Sm-146, an important isotope for early solar system chronometry. Similarly, we have been in discussions with Morgan White at LANL about using MMCs to accurately measure the total kinetic energy (TKE) of fission in Cf-252, a crucial reference material for calibration of neutron detectors and neutron multiplicity. For NDA, I expect MMCs initially to be most useful for improving the underlying nuclear data, which we know are often limiting the accuracy. Once better data are available, I expect MMCs to provide an MMC accuracy comparable to current DA by mass spectrometry.

Most importantly for nuclear safeguards, after years of discussions, the **IAEA has requested tests of cryogenic detectors for high-accuracy isotope measurements**, specifically for very small particles where mass spectrometry is difficult. This has led to a follow-up project with NA-241 to adapt MMCs for **decay energy (Q) spectroscopy**, where the actinide particle is fully enclosed inside and absorber so that all decay products deposit the entire energy of the decay inside the MMC. This ensures 100% detection efficiency and produces a single peak per isotope at the Q-value of its decay. We are currently preparing an SP-1 proposal with the IAEA to test MMCs in this application with certified reference materials and with IAEA inspection samples. If successful, LLNL and LANL will provide a cryogenic Q-spectrometer based on MMC and/or TES microcalorimeters to the IAEA NML in FY23

Since microcalorimeters measure the heat deposited by a particle interaction, it is also very likely that MMC detectors will be adapted for other types of radiation. MMC use in the search for a **neutrino-less double-beta decay** is a high-profile science experiment in Korea. At LLNL, we are considering MMC ion detectors for use at the Center for **Accelerator Mass Spectrometry** to improve the detectability for **very rare isotopes** such as U-236 in the context of nuclear forensics. Similarly, LBNL is interested in MMCs for experiments with **super-heavy elements**. I am quite confident that many other applications for MMCs will emerge, especially where they provide an advantage over superconducting transition edge sensor (TES) γ-detectors because of their higher linearity and reproducibility.

My experience has been that some of the best measurements with the various cryogenic detector technologies we have developed grew out of chance encounters with users who had urgent scientific or programmatic questions that they thought we might be able to help them with. The best way to facilitate these encounters is to continue to advance MMC technology, use it for high-impact measurements and present them at the various meetings or in publications where they will be noticed. That's exactly what we hope to do.

Appendix A

List of Publications

[Bates 2016a] "Direct Detection of Pu-242 with a Metallic Magnetic Calorimeter Gamma-Ray Detector", C. Bates, C. Pies, S. Kempf, D. Hengstler, A. Fleischmann, L. Gastaldo, C. Enss, S. Friedrich, *J. Low Temp. Phys*. **184**, 351–355 (2016)

[Bates 2016b] "Reproducibility and Calibration of MMC-Based High-Resolution Gamma Detectors", C. R. Bates, C. Pies, S. Kempf, D. Hengstler, A. Fleischmann, L. Gastaldo, C. Enss, S. Friedrich, *Appl. Phys. Lett.* **109**, 023513 (2016)

[Boyd 2018] "Integrated SQUID/Sensor Metallic Magnetic Microcalorimeter for Gamma-Ray Spectroscopy", S. T. P. Boyd, R. Hummatov, G. B. Kim, J. A. Hall, R. Cantor, S. Friedrich, *J. Low Temp. Phys*. **193**, 435-440 (2018)

[Boyd 2020] "Metallic Magnetic Calorimeters for High-Accuracy Nuclear Decay Data", S. T. P. Boyd, G.-B. Kim, J. A. Hall, R. H. Cantor, S. Friedrich, *J. Low Temp. Phys*. 199, 681–687 (2020)

[Friedrich 2018] "Magnetic Microcalorimeter Gamma Detectors for High-Accuracy Nuclear Decay Data", S. Friedrich, G.-B. Kim, R. Hummatov, T. Parsons-Davis, R. Cantor, S. Boyd, *Proceedings of the 51st Annual Meeting of the Institute of Nuclear Materials Management,* Baltimore (2018)

[Hummatov 2017] "Tantalum Passive Persistence Shunts for On-Chip Current Trapping in Metallic Magnetic Calorimetry", R. Hummatov, L. N. Le, J. A. Hall, S. Friedrich, R. A. Cantor, S. T. P. Boyd, *IEEE Trans. Appl. Supercond*. **27**, 2200205 (2017)

[Hummatov 2018] "Fabrication of High-Resolution Gamma-Ray MMCs with AgEr Sensor and Thick Electroplated Absorbers", R. Hummatov, J. A. Hall, G.-B. Kim, S. Friedrich, R. Cantor, S. T. P. Boyd, *J. Low Temp. Phys*. **193**, 752-757 (2018)

[Jaeckel 2012] "Dedicated Co-deposition System for Metallic Paramagnetic Films" F. Jaeckel, V. Kotsubo, J.A. Hall, R. Cantor, S.T.P. Boyd, *J. Low Temp. Phys*. **167**, 286–291 (2012)

[Kim 2018a] "Development of MMC Gamma Detectors for Precise Characterization of Uranium Isotopes", G.-B. Kim, C. C. Flynn, S. Kempf, L. Gastaldo, A. Fleischmann, C. Enss, S. Friedrich, *J. Low Temp. Phys*. **193**, 1236-1242 (2018)

[Kim 2018b] "Consistent measurements of ^{233}U gamma emissions using metallic magnetic calorimeters with ultra-high energy resolution", G.-B. Kim, R. Hummatov, S. Kempf, C. Flynn, R. Cantor, A. Fleischmann, S. T. P. Boyd, C. Enss, S. Friedrich, *J. Radioanal. Nucl. Chem*. **318**, 803-808 (2018)

[Kim 2020] "A New Measurement of the 60 keV Emission from Am-241 Using Metallic Magnetic Calorimeters", G. B. Kim, S. T. P. Boyd, R. H. Cantor, A. S. Voyles, J. T. Morrell, L. A. Bernstein, S. Friedrich, *J. Low Temp. Phys.* (2020)